



Major element and primary sulfur concentrations in Apollo 12 mare basalts: The view from melt inclusions

Daniel J. BOMBARDIERI^{1*}, Marc D. NORMAN², Vadim S. KAMENETSKY¹, Leonid V. DANYUSHEVSKY¹

¹Centre for Ore Deposit Research, School of Earth Sciences, University of Tasmania, Hobart TAS 7001, Australia

²Research School of Earth Sciences, The Australian National University, Canberra 0200, Australia

*Corresponding author. E-mail: Daniel.Bombardieri@aad.gov.au

(Received 23 August 2004; revision accepted 28 March 2005)

Abstract—Major element and sulfur concentrations have been determined in experimentally heated olivine-hosted melt inclusions from a suite of Apollo 12 picritic basalts (samples 12009, 12075, 12020, 12018, 12040, 12035). These lunar basalts are likely to be genetically related by olivine accumulation (Walker et al. 1976a, b). Our results show that major element compositions of melt inclusions from samples 12009, 12075, and 12020 follow model crystallization trends from a parental liquid similar in composition to whole rock sample 12009, thereby partially confirming the olivine accumulation hypothesis. In contrast, the compositions of melt inclusions from samples 12018, 12040, and 12035 fall away from model crystallization trends, suggesting that these samples crystallized from melts compositionally distinct from the 12009 parent liquid and therefore may not be strictly cogenetic with other members of the Apollo 12 picritic basalt suite. Sulfur concentrations in melt inclusions hosted in early crystallized olivine (Fo_{75}) are consistent with a primary magmatic composition of 1050 ppm S, or about a factor of 2 greater than whole rock compositions with 400–600 ppm S. The Apollo 12 picritic basalt parental magma apparently experienced outgassing and loss of S during transport and eruption on the lunar surface. Even with the higher estimates of primary magmatic sulfur concentrations provided by the melt inclusions, the Apollo 12 picritic basalt magmas would have been undersaturated in sulfide in their mantle source regions and capable of transporting chalcophile elements from the lunar mantle to the surface. Therefore, the measured low concentration of chalcophile elements (e.g., Cu, Au, PGEs) in these lavas must be a primary feature of the lunar mantle and is not related to residual sulfide remaining in the mantle during melting. We estimate the sulfur concentration of the Apollo 12 mare basalt source regions to be ~75 ppm, which is significantly lower than that of the terrestrial mantle.

INTRODUCTION

Inferring the primary characteristic of parental magmas from igneous cumulates is a continuing challenge. The composition of a cumulate rock is, by definition, significantly removed from that of the melt from which it formed, so primary magmatic characteristics must be recovered indirectly. Geochemical and petrological studies of melt inclusions trapped within cumulate crystals offer one approach to understanding the petrogenesis of cumulate rocks. Melt inclusions represent small parcels of melt that have been trapped by growing crystals and thus provide a “snapshot” of a particular evolutionary phase of a magma (Roedder 1979; Sobolev 1996). However, the information contained within polycrystalline melt inclusions such as those

typical of cumulate rocks is complicated and often difficult to decipher. Weiblen (1977) summarized defocused beam electron microprobe data for polycrystalline melt inclusions from lunar mare basalts and showed that compositions of these inclusions indicate a more complicated petrogenesis than is apparent from whole rock studies, although uncertainties introduced by non-representative sampling of individual polycrystalline melt inclusions compromised their ability to define the liquid line of descent.

More direct information about the composition of trapped melt can be obtained by performing homogenization experiments on polycrystalline melt inclusions (Fig. 1e) to produce a glass suitable for microbeam chemical analysis (Figs. 1c, d, f). This allows for precise measurements by electron microprobe on melt inclusions as small as 10

microns. However, even this approach is not always straightforward as primary compositions of melt inclusions can be modified by post-entrapment processes such as diffusive Fe loss, quench crystallization, and volatile dissociation (e.g., Danyushevsky et al. 2002). Incautious interpretation of compositional data from homogenized melt inclusions affected by post entrapment modification can lead to erroneous conclusions regarding magmatic compositions and trapping temperatures (Danyushevsky et al. 2002). Fortunately, such effects can usually be circumvented through corrections to the data (Danyushevsky et al. 2000, 2002).

We have studied a suite of olivine-hosted melt inclusions from Apollo 12 picritic olivine basalts in order to improve our understanding of the petrogenesis of these lavas and the composition of the lunar mantle. The petrography and major element compositions of this suite of low-Ti basalts can be related by olivine accumulation in a thick flow (Walker et al. 1976a, b). Therefore, studies of olivine-hosted melt inclusions from this suite provide the opportunity to examine the magmatic evolution of a low-Ti mare lava flow from a new perspective.

The first goal of this study is to evaluate the olivine accumulation model proposed by Walker et al. (1976a) by comparing the liquid line of descent implied by the major element compositions of melt inclusions with model trends for a fractionating Apollo 12 olivine basalt parental magma. The second goal is to place better constraints on the primary S contents of Apollo 12 low-Ti olivine basalts. Mare lavas are thought to have rapidly degassed, losing sulfur and other volatiles during their transit through the lunar crust and eruption into the hard vacuum of space (Weitz et al. 1999). Therefore, measured whole rock S concentrations provide only lower limits for the primary S concentrations of mare basalts, whereas melt inclusions trapped in early crystallized olivine may provide better sulfur estimates of the undegassed magma. Such data bear directly on the question of sulfide saturation in the mantle source regions responsible for generation of mare basalts. This study compares sulfur concentrations of homogenized melt inclusions with whole rock and experimental data in order to evaluate the possibility of sulfide saturation in the lunar mantle during the formation of Apollo 12 parental magmas. If primary sulfur concentrations were sufficiently high to induce sulfide saturation during melting, concentrations of chalcophile elements in the lunar mantle may be more abundant than is commonly thought. Therefore, studies such as this have the potential to provide new information on the state of the lunar interior and the chalcophile element concentration of the Moon.

SAMPLE PREPARATIONS AND METHODS

For our initial study, we selected six thin section samples of Apollo 12 olivine basalts (samples 12009, 12075, 12020,

12018, 12040, 12035) representing the range of petrographic and major element variations for this suite of lavas. Our observations confirmed the abundance of polycrystalline melt inclusions 15 to 100 μm in size contained within olivine phenocrysts. The melt inclusions occur as ellipsoid and irregular shapes. Naturally quenched melt inclusions in mare basalts are nearly always polycrystalline and rarely found as glass, indicating cooling rates sufficiently slow to permit nucleation and growth of one or more crystalline phases. Polycrystalline melt inclusions in Apollo 12 olivine basalts consist of pyroxene, Cr spinel, feldspar, ilmenite, rare sulfides and a shrinkage bubble (Fig. 1a, b, e).

Following our preliminary investigations of thin sections, we were allocated a total of 1.2 g of material (each sample weighed approximately 200 mg) from the NASA Planetary Materials Curators Office at the Johnston Space Center, Houston. Using a pestle and mortar we carefully crushed the samples and then sieved the particulates using 0.5, 0.7, and 1 mm plastic mesh. From each size fraction we chose olivine grains containing suitable melt inclusions for homogenization experiments (i.e. melt inclusions wholly contained within the host crystal). In total, forty olivine grains 250–700 microns in size, with suitable melt inclusions were selected for homogenization experiments.

To conduct our melting experiments, we used a high-temperature heating stage housed at the melt inclusion laboratory, Center for Ore Deposit Research, University of Tasmania. The apparatus is a micro-heater assembly consisting of a Pt tube ($\text{Pt}_{90}\text{Rh}_{10}$) 2 mm in diameter and 6 mm in length. The sample holder comprises a platinum ring 1 mm in diameter, located in the center of the heater. A $\text{Pt}_{90}\text{-Rh}_{10}$ thermocouple, which is welded to the sample holder, monitored the temperature during the experiment (see Sobolev et al. 1980 for complete description of the heating stage apparatus). Experimental studies of Apollo 12 olivine basalts (Green et al. 1971; Walker et al. 1976b) were used as a guide to estimate the likely range of homogenization temperatures (1050 °C to 1300 °C, equivalent to Fo_{50-75} , respectively). We began our experiments by heating the olivine grains to 1100 °C at a rate of 200 °C/min. Above 1100 °C, the grains were heated between 50 °C to 25 °C/min until the inclusion melted and held at this temperature for approximately one minute. The grains were quenched rapidly by flushing helium through the sample chamber. Each olivine grain was mounted in epoxy and polished individually to expose the homogenized melt inclusion for electron microprobe analysis.

Concentrations of major elements and sulfur were measured in glass and sulfide globules within melt inclusions, using a Cameca SX-50 electron microprobe at the University of Tasmania's Central Science Laboratory (C. S. L). Major element compositions of host olivine for each melt inclusion were also measured. Where possible, replicate analyses of melt inclusions were undertaken and the results averaged. We

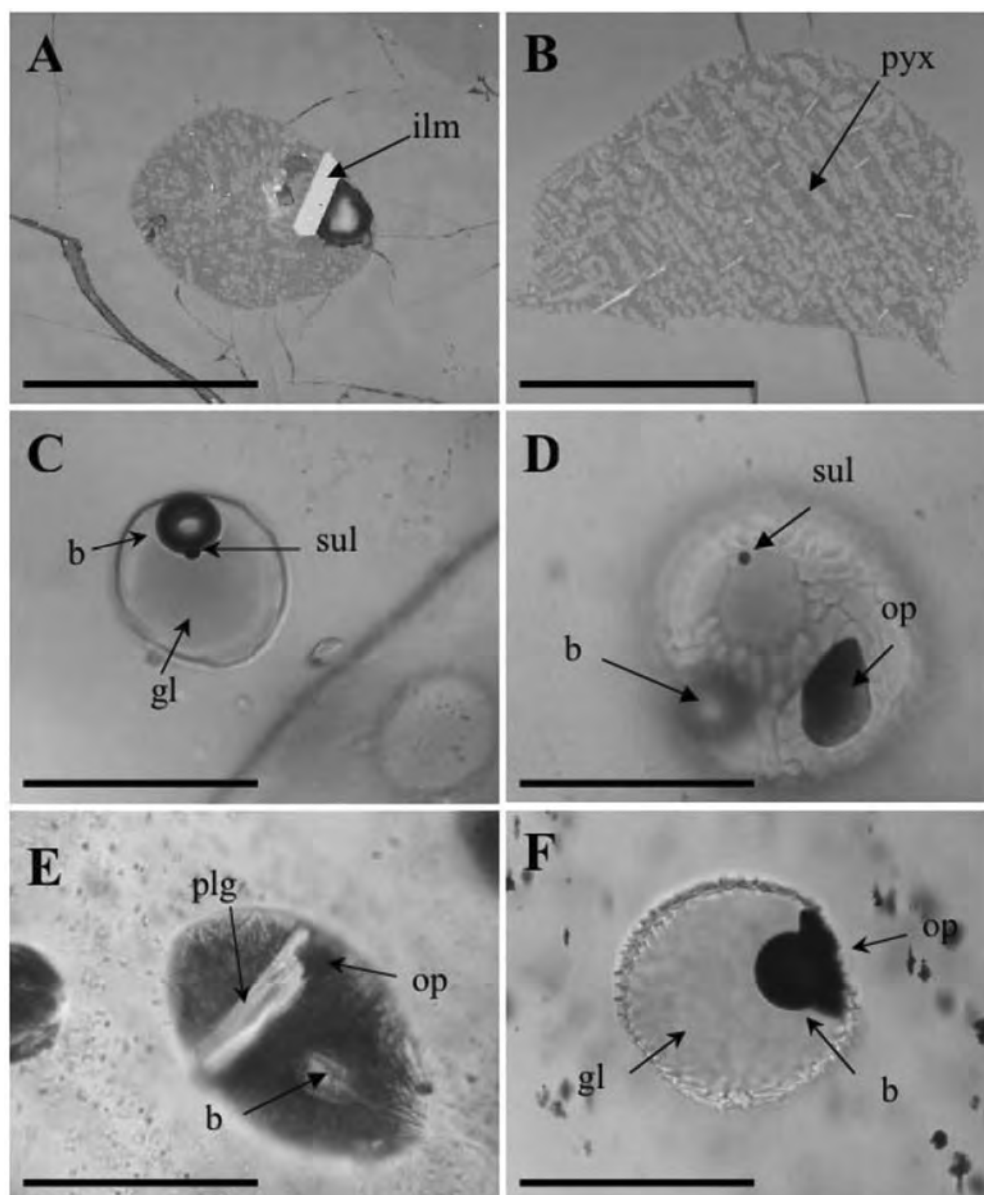


Fig. 1. Photomicrographs of melt inclusions: a) Naturally quenched melt inclusion from sample 12040 showing dendritic pyroxene, a large grain of ilmenite, and shrinkage bubble in a matrix of evolved glass; b) Naturally quenched inclusion from 12075 showing dendritic pyroxene and thin ilmenite laths in a glass matrix; c) Experimentally melted inclusions 12075-1 quenched to glass (gl). A small sulfide globule (sul) is attached to the bubble (b). d) Experimentally melted inclusion 12075-6a showing “orange skin” appearance interpreted as due to overheating. A relict Cr spinel grain (op), sulfide globule (sul) and shrinkage bubble (b) are present. e) Naturally quenched melt inclusion from sample 12018 showing dendritic pyroxene matrix, relict Cr spinel grain (op), a large grain of plagioclase feldspar (plg), and shrinkage bubble (b). f) Experimentally melted inclusion 12035-1 quenched to glass showing relict Cr spinel grain (op), and shrinkage bubble (b). (a) and (b) in reflected light; (c), (d), (e) and (f) in transmitted light. Scale bar is 40 microns in (a), (b), (c), (e), and (f), and 20 microns in (d).

chosed marcassite and troilite (both FeS) as the primary calibration standards for S analyses in glass and sulfide, respectively, and a basaltic glass standard (VG-2) was analyzed during each session for quality control (Table 1). Dissolved sulfur concentrations were measured in glass by integrating the entire S X-ray peak in 19 step intervals. At each step interval the intensity was measured for 25 sec (i.e., a total counting time of 8 minutes per analysis). This procedure produced a detection limit for S of ~25 ppm.

RESULTS

Petrography and Major Element Compositions of Experimentally Heated Melt Inclusions

Experimentally heated melt inclusions are composed of glass and a shrinkage bubble, and may contain Cr spinel and/or a sulfide globule (Fig. 1d). Most of the Cr spinel was trapped within the growing olivine phenocryst during

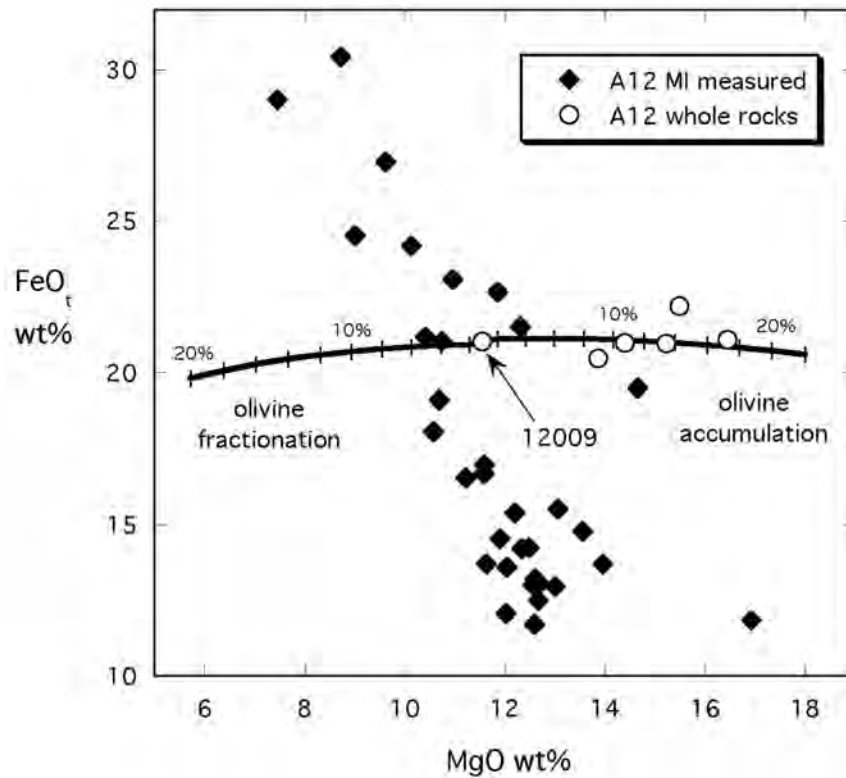


Fig. 2. Diagram showing evidence for post-entrapment modification (diffusive Fe loss) and overheating in melt inclusions. Measured FeO_t concentrations in melt inclusions are substantially lower (down to ~11.5%) compared with whole rock (~21 wt%; Papike et al. 1999) and modelled olivine fractionation and accumulation trends (~21 to 17 wt%). Melt inclusions with elevated FeO_t contents of up to 30 wt% may be attributed to melting of host olivine components during experimental heating.

Table 1. EMPA analyses of VG2^a reference materials.

	wt%	Mean (n = 7)	S. D.
SiO_2	50.81	51.08	± 0.09
TiO_2	1.85	1.98	± 0.04
Al_2O_3	14.06	14.13	± 0.05
FeO^b	11.84	11.78	± 0.18
MnO	0.22	0.22	± 0.04
MgO	6.71	6.78	± 0.06
CaO	11.12	10.89	± 0.15
Na_2O	2.62	2.53	± 0.05
K_2O	0.19	0.20	± 0.01
P_2O_5	0.20	0.22	± 0.04
Total	99.62	99.80	

^aVG2: basaltic glass, Juan de Fuca Ridge, USNM 111240/52 (Jarosewich et al. 1979).

^bAll Fe as FeO.

crystallization. This is supported by phase equilibrium experiments, which are consistent with co-crystallization of Cr spinel and olivine during the early evolution of these magmas (Green et al. 1971). Some melt inclusions showed visible signs of decrepitation possibly resulting from syn- or post-eruptive rupture of the host olivine during experimental heating. Visible evidence for compromised melt inclusions includes fractures or melt ribbons intersecting the melt inclusion, and the large size of the shrinkage bubble relative

to the size of the inclusion. Compromised melt inclusions were not included in this study because their major element and especially their volatile concentrations may differ significantly from their original composition.

Major Elements: Measured Compositions

Major element compositions of experimentally heated melt inclusions differ significantly from the whole rock compositions of Apollo 12 olivine basalts. Many melt inclusions contain substantially lower FeO_t concentrations (11.0 to 18.0 wt%, where FeO_t = total Fe calculated as FeO), compared to the whole rocks (20.5 to 22.5 wt% FeO_t ; Fig. 2). Low FeO_t concentrations are attributed to post entrapment loss of Fe from the melt inclusion through olivine crystallization on the wall of the melt inclusion and Fe-Mg exchange between the trapped melt and host olivine (Danyushevsky et al. 2000). In contrast, some melt inclusions in relatively evolved olivine contain substantially elevated FeO_t concentrations (23.0 to 30.5 wt%) compared to whole rock concentrations. This may be an experimental artefact of overheating (e.g., melting of host olivine components) or perhaps it indicates a more complex petrogenesis in which these olivines were entrained by a higher temperature melt after the inclusions were trapped.

Table 2a. Measured and corrected major element and sulfur contents of experimentally heated Apollo 12 olivine-hosted melt inclusions.

Sample	Cr spinel	SiO ₂	TiO ₂	Al ₂ O ₃	FeO _t	MnO	MgO	CaO	Na ₂ O	K ₂ O	P ₂ O ₅	Cr ₂ O ₃	S ¹	Total	mg#	Kd	MI (μm)	Fo host	T (°C)
12009MI-1a	M	46.96	4.29	10.64	14.53	0.21	11.90	10.63	0.35	0.18	0.20	0.40	0.1053	100.38	59.35	0.51			
	C	44.78	3.76	9.32	20.95	0.18	10.71	9.31	0.31	0.16	0.18	0.35	n.d.	100.01	47.67	0.32	44	73.98	1261
12075MI-1	M	48.42	3.49	11.04	12.05	0.14	12.03	11.44	0.28	0.07	0.09	0.59	0.0722	99.72	64.00	0.58			
	C	45.34	2.82	8.93	21.03	0.11	11.66	9.26	0.23	0.06	0.07	0.48	0.0876	100.08	49.70	0.32	36	75.34	1282
12075MI-2	M	47.85	2.93	10.23	15.38	0.24	12.20	10.62	0.23	0.05	0.07	0.35	0.0879	100.23	58.56	0.51			
	C	45.97	2.65	9.24	20.96	0.22	10.73	9.59	0.21	0.05	0.06	0.32	n.d.	100.00	47.71	0.33	33	73.47	1261
12075MI-3	M	48.72	3.36	10.70	13.05	0.16	12.70	10.82	0.28	0.07	0.09	0.40	0.1044	100.45	63.42	0.59			
	C	45.79	2.84	9.04	20.99	0.14	11.36	9.14	0.24	0.06	0.08	0.34	n.d.	100.02	49.09	0.33	46	74.66	1276
12075MI-4	M	48.04	3.20	10.15	13.70	0.18	13.96	10.48	0.23	0.06	0.08	0.53	0.0668	100.68	64.49	0.62			
	C	45.57	2.85	9.03	20.95	0.16	11.31	9.32	0.20	0.05	0.07	0.47	n.d.	99.98	49.03	0.33	40	74.68	1274
12075MI-6a	M	47.04	2.87	10.03	16.76	0.28	11.59	10.20	0.20	0.06	0.10	0.77	0.0917	100.00	55.21	0.46			
	C	45.75	2.66	9.31	20.96	0.26	10.53	9.47	0.19	0.06	0.09	0.71	0.0920	100.08	47.24	0.33	26	72.99	1255
12075MI-6b	M	47.54	2.98	9.73	15.52	0.19	13.06	10.17	0.23	0.06	0.08	0.96	0.0890	100.61	60.00	0.54			
	C	45.71	2.75	8.97	20.96	0.18	10.82	9.38	0.21	0.06	0.07	0.89	n.d.	100.00	47.91	0.33	16	73.62	1262
12020MI-3	M	48.36	2.87	9.83	14.78	0.16	13.56	9.88	0.23	0.06	0.07	0.54	0.0845	100.05	62.05	0.66			
	C	46.64	2.73	9.35	20.89	0.15	9.98	9.39	0.22	0.06	0.07	0.51	n.d.	100.08	45.65	0.34	60	71.35	1242
12020MI-4	M	48.42	2.85	10.43	14.24	0.20	12.48	10.46	0.23	0.04	0.06	0.69	0.0616	100.16	60.96	0.60			
	C	46.31	2.57	9.42	20.96	0.18	10.17	9.45	0.21	0.04	0.05	0.62	n.d.	99.98	46.37	0.33	25	72.08	1248
12020MI-6a	M	48.75	3.21	10.44	12.95	0.11	13.01	10.63	0.24	0.07	0.07	0.57	0.0567	100.10	64.16	0.66			
	C	46.18	2.82	9.16	20.98	0.10	10.60	9.32	0.21	0.06	0.06	0.50	0.0846	100.07	47.38	0.33	35	73.06	1258
12020MI-6b	M	49.03	3.29	10.44	13.22	0.19	12.60	10.75	0.24	0.07	0.11	0.53	0.0626	100.52	62.94	0.60			
	C	46.10	2.80	8.90	20.99	0.16	11.06	9.16	0.20	0.06	0.09	0.45	0.0921	100.06	48.43	0.33	38	73.94	1268
12020MI-8b	M	48.64	2.90	9.89	16.53	0.21	11.23	10.12	0.23	0.07	0.09	0.15	0.0918	100.16	54.76	0.42			
	C	47.25	2.20	8.63	21.00	0.19	11.37	8.80	0.21	0.06	0.09	0.20	n.d.	100.00	49.10	0.34	40	74.03	1273
12020MI-9a	M	49.33	3.36	10.87	12.48	0.15	12.67	10.90	0.26	0.07	0.09	0.51	0.0476	100.74	64.40	0.63			
	C	46.01	2.80	9.07	20.96	0.13	11.16	9.09	0.22	0.06	0.08	0.43	0.0680	100.08	48.69	0.33	39	74.19	1270
12020MI-9b	M	49.27	3.12	10.74	12.99	0.19	12.57	10.72	0.24	0.07	0.10	0.65	0.0721	100.73	63.29	0.63			
	C	46.24	2.67	9.20	20.95	0.16	10.68	9.18	0.21	0.06	0.09	0.56	n.d.	100.00	47.60	0.33	29	73.13	1259
12020MI-9c	M	49.45	2.69	11.01	13.70	0.21	11.63	10.98	0.25	0.03	0.05	0.80	0.0787	100.88	60.20	0.56			
	C	46.34	2.27	9.29	20.98	0.18	10.73	9.26	0.21	0.03	0.04	0.67	n.d.	100.00	47.68	0.33	15	73.13	1260

Abbreviations: * = melt inclusions which contain Cr-spinel, n.d. = Cr-spinel or sulfide not detected; M = measured melt inclusion composition; C = calculated initial trapped melt composition according to the procedure of Danyushevsky et al. (2000); T = calculated olivine liquidus temperature. Temperatures are calculated for dry conditions at 1 atm. using the model of Ford et al. (1983); FeO_t calculated as FeO (assuming no Fe₂O₃); S¹ = total S calculated using mass balance.

Table 2b. Measured and corrected major element and sulfur contents of experimentally heated Apollo 12 olivine-hosted melt inclusions.

Sample	Cr spinel	SiO ₂	TiO ₂	Al ₂ O ₃	FeO _t	MnO	MgO	CaO	Na ₂ O	K ₂ O	P ₂ O ₅	Cr ₂ O ₃	S ¹	Total	mg#	Kd	MI (μ m)	Fo host	T (°C)
12020MI-9d	M	49.62	2.78	11.05	13.59	0.15	12.04	10.73	0.26	0.06	0.12	0.76	0.0660	101.22	61.20	0.57	18	73.48	1265
	C	46.32	2.34	9.30	20.96	0.13	10.92	9.03	0.22	0.05	0.10	0.64	n.d.	100.01	48.14	0.34	18	73.48	1265
12020MI-9e	M	48.65	3.21	10.77	14.20	0.24	12.34	10.90	0.25	0.06	0.04	0.64	0.1017	101.39	60.76	0.61	22	71.64	1240
	C	45.94	2.86	9.59	20.95	0.21	9.86	9.70	0.22	0.05	0.04	0.57	n.d.	99.99	45.61	0.33	22	71.64	1240
12018MI-1	M	52.45	1.74	8.96	11.70	0.14	12.59	11.28	0.34	0.09	0.11	0.81	0.0480	100.26	65.73	0.74	29	72.26	126
	C	48.71	1.46	7.52	20.96	0.12	10.64	9.46	0.29	0.08	0.09	0.68	n.d.	100.01	47.50	0.35	29	72.26	126
12018MI-5b	M	50.09	2.19	9.38	16.93	0.22	11.84	9.66	0.23	0.06	0.09	0.67	0.0619	101.43	55.48	0.69	26	64.32	1176
	C	49.34	2.28	9.76	19.97	0.23	7.26	10.05	0.24	0.06	0.09	0.70	n.d.	99.98	39.31	0.36	26	64.32	1176
12040MI-7a	M	48.64	2.59	7.65	18.06	0.32	10.58	10.93	0.23	0.07	0.08	0.72	0.0618	99.94	51.07	0.65	37	59.6	1145
	C	49.61	2.81	8.31	19.93	0.35	6.36	11.88	0.25	0.08	0.09	0.78	0.0863	100.54	36.25	0.35	37	59.6	1145
12040MI-7b	M	48.52	2.91	9.51	16.97	0.22	11.60	9.81	0.30	0.07	0.10	0.60	0.0811	100.71	54.91	0.84	24	61.67	1150
	C	49	3.28	10.72	18.98	0.25	5.49	11.06	0.34	0.08	0.11	0.68	n.d.	100.07	34.01	0.36	24	61.67	1150
12040MI-7c	M	47.64	3.10	9.08	19.11	0.21	10.69	9.40	0.29	0.06	0.05	0.66	0.1059	100.39	49.93	0.66	30	60.21	1128
	C	48.86	3.59	10.51	18.97	0.24	5.72	10.88	0.34	0.07	0.06	0.76	n.d.	100.11	34.95	0.36	30	60.21	1128
12040MI-8	M	45.88	2.37	7.88	24.19	0.26	10.13	8.65	0.24	0.05	0.09	0.55	0.0977	100.40	42.74	0.60	29	55.44	1100
	C	49.31	3.17	10.55	18.97	0.35	4.80	11.59	0.32	0.07	0.12	0.74	n.d.	100.09	31.08	0.36	29	55.44	1100
12035MI-1	M	48.12	1.51	6.98	19.50	0.20	14.66	8.04	0.23	0.06	0.08	0.69	0.0848	100.15	57.26	0.78	46	63.18	1173
	C	50.43	1.92	8.85	19.96	0.25	7.03	10.20	0.29	0.08	0.10	0.88	0.0848	100.07	38.56	0.37	46	63.18	1173
12035MI-2a	M	46.19	2.46	8.31	21.53	0.23	12.32	8.50	0.25	0.07	0.08	0.74	0.0959	100.77	50.49	0.77	55	56.91	1107
	C	48.71	3.25	10.98	18.95	0.30	5.05	11.23	0.33	0.09	0.11	0.98	0.0959	100.08	32.20	0.36	55	56.91	1107
12035MI-2b	M	46.18	2.40	8.20	22.66	0.25	11.86	8.12	0.21	0.08	0.07	0.40	0.0888	100.52	48.25	0.70	33	51.5	1072
	C	49.31	3.24	11.05	18.95	0.34	5.13	10.95	0.28	0.11	0.09	0.54	0.0888	100.08	32.54	0.36	33	51.5	1072
12035MI-2c	M	46.52	2.26	8.07	23.08	0.22	10.96	8.44	0.22	0.06	0.04	0.71	0.0821	100.67	45.83	0.63	45	57.37	1113
	C	49.52	2.97	10.60	18.97	0.29	5.21	11.09	0.29	0.08	0.05	0.93	0.0821	100.08	32.86	0.36	45	57.37	1113
12035MI-3a	M	45.39	2.81	7.16	26.98	0.29	9.62	7.38	0.25	0.04	0.03	0.48	0.0987	100.52	38.86	0.60	20	46.51	1049
	C	50.58	4.18	10.66	17.99	0.43	3.97	10.98	0.37	0.06	0.04	0.71	0.0987	100.07	28.23	0.37	20	46.51	1049
12035MI-3b	M	46.24	2.44	7.06	29.03	0.32	7.46	6.96	0.26	0.05	0.10	0.34	0.1206	100.37	31.41	0.53	29	59.97	1127
	C	53.04	3.72	10.77	17.00	0.49	3.22	10.62	0.40	0.08	0.15	0.52	0.1206	100.13	25.24	0.39	29	59.97	1127
12035MI-4	M	47.00	3.56	7.59	21.19	0.21	10.41	8.85	0.26	0.05	0.08	0.71	0.1004	100.01	46.68	0.58	35	58.7	1113
	C	49.3	4.35	9.28	18.96	0.26	5.68	10.82	0.32	0.06	0.10	0.87	0.1004	100.10	34.80	0.36	35	58.7	1113
12035MI-5	M	46.08	3.39	8.10	21.05	0.23	10.75	9.43	0.28	0.06	0.06	0.61	0.0879	100.13	47.64	0.64	20	53.71	1094
	C	48.2	4.21	10.05	19.00	0.29	5.30	11.70	0.35	0.07	0.07	0.76	0.0879	100.09	33.20	0.35	20	53.71	1094
12035MI-6	M	47.80	3.20	7.68	24.54	0.21	9.02	7.22	0.38	0.09	0.08	0.49	0.0864	100.79	39.56	0.56	44	51.51	1046
	C	51.86	4.27	10.24	17.96	0.28	4.38	9.62	0.51	0.12	0.11	0.65	0.0864	100.09	30.29	0.37	44	51.51	1046
12035MI-28	M	42.78	2.94	6.44	30.45	0.32	8.72	7.66	0.20	0.04	0.10	0.36	0.0774	100.09	33.79	0.48	44	51.51	1046
	C	49.19	4.92	10.77	16.96	0.54	3.63	12.81	0.33	0.07	0.17	0.60	0.0774	100.07	27.61	0.36	44	51.51	1046

Abbreviations as in Table 3.

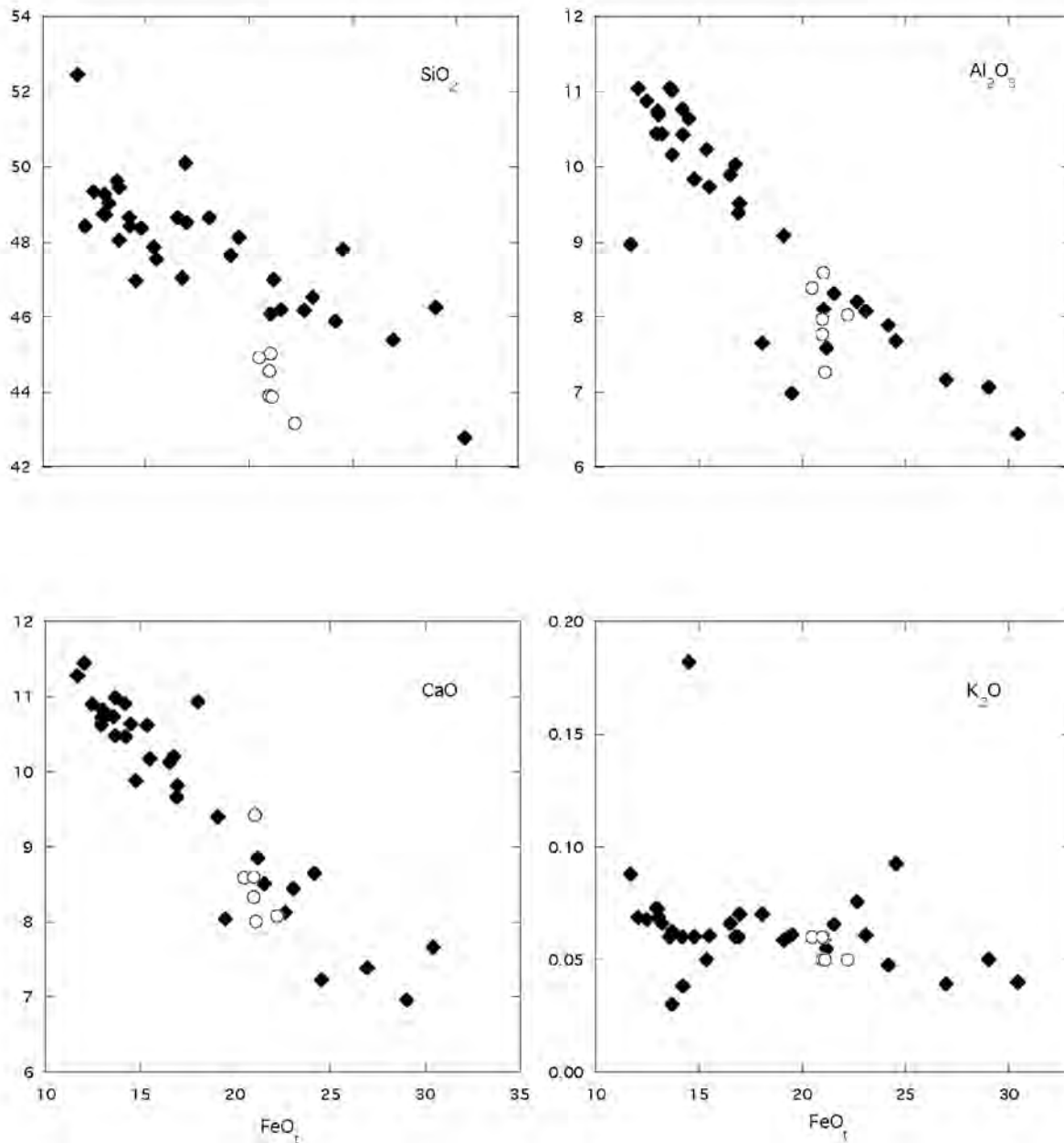


Fig. 3. Measured compositions of uncorrected olivine hosted melt inclusions (solid black diamonds) from the Apollo 12 olivine basalt suite (12009, 12075, 12020, 12018, 12040, and 12035) plotted as oxides versus FeO, compared with whole rock compositions for this suite (open circles).

SiO₂ concentrations in melt inclusions (Fig. 3) are somewhat higher (46.0 to 53.0 wt%) than the whole rock concentrations of these lavas (43.2 to 45.0 wt%). Our data for SiO₂ in the VG2 glass standard shows good precision and close agreement with established values (Table 1), so it is unlikely that the higher SiO₂ concentrations measured in these melt inclusions are analytical artefacts. CaO and Al₂O₃ concentrations (7 to 11 wt% and 6.5 to 11.5 wt%, respectively) are somewhat more variable compared to whole rock equivalents (8 to 9.5 wt% and 7.5 to 8.5 wt%, respectively), whereas TiO₂ and Cr₂O₃ concentrations

(0.9 wt% to 5.4 wt% and 0.15 to 1.15 wt%, respectively) show very large variations compared to the whole rocks (2.3 to 2.9 wt% and 0.49 to 0.63 wt%). Concentrations of K₂O, P₂O₅ and Na₂O in most melt inclusions are slightly elevated compared to whole rock concentrations, however, for a small number of melt inclusions, concentrations of these elements are elevated by almost a factor of ten compared to whole rock equivalents.

Host olivine compositions analyzed 50–100 μm from the melt inclusions have the range Fo₄₆–Fo₇₅. Melt inclusions hosted in early crystallized olivine (Fo₇₀–Fo₇₅), are expected

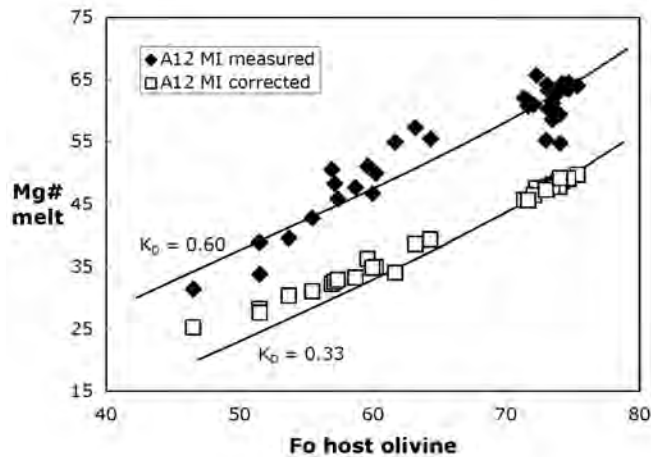


Fig. 4. Mg# (Mg/Mg+Fe atomic) of experimentally heated melt inclusions compared to forsterite (Fo) composition of their host olivine. $K_D = 0.60$ and 0.33 are lines of constant K_D . High $K_D \geq 0.40$ of experimentally melted inclusions indicate that as measured they do not directly represent trapped equilibrium melts. Melt inclusion compositions corrected according to the procedure of Danyushevsky et al. (2000), assuming 17 to 21 wt% FeO content in the melt, and oxygen fugacity at 2 log units below the iron-wüstite (IW) buffer (filled circles) show a more restrictive range of K_D 's that are close to the expected equilibrium values (0.33 and 0.39).

to provide the best approximation of the major element composition of the parental magma and the primary S concentration of the Apollo 12 olivine basalt suite. In contrast, melt inclusions hosted in more evolved olivine (Fo_{69} to Fo_{46}) should give insights into the liquid line of descent as well as the volatile history of mare lavas toward the later stage of their evolution. Major element partitioning relations were used to test whether compositions of experimentally heated melt inclusions were in equilibrium with their host olivine at the conditions of the experiment. Fe-Mg partitioning shows that the experimentally melted inclusions do not directly represent the compositions of melts in equilibrium with their host olivine at the time of trapping (K_D 0.44 to 0.77; Fig. 4). This was expected due to the relatively rapid heating rates used in the experiments and the limited time (~1 minute) allowed for melt inclusions to equilibrate with the host olivine during the melting experiment. There is also evidence for overheating, particularly for olivine-hosted melt inclusions from samples 12035 and 12040 (Fig. 5).

Corrections to Melt Inclusion Compositions

The effects of underheating and overheating and possible associated Fe-Mg exchange with the host were corrected using a computer program (FeO_Eq2.exe; Danyushevsky et al. 2000). This correction reconstructs the initial trapped melt composition from the composition of the residual melt by adding or removing olivine from the host, and by substituting Fe for Mg in the inclusion until it is in equilibrium with its

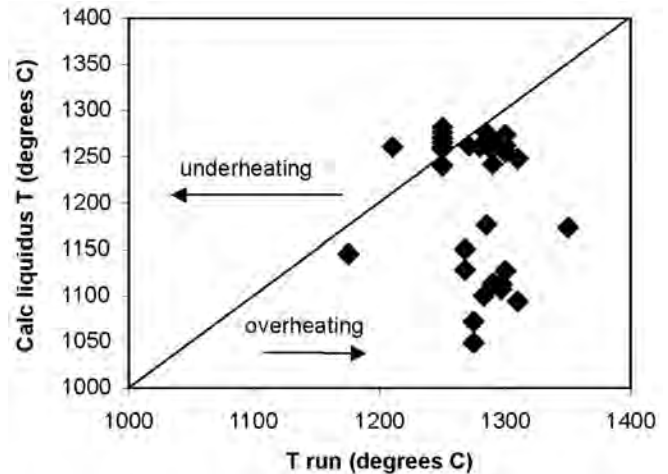


Fig. 5. Dry liquidus temperatures for melt inclusions calculated from their host olivine compositions compared to the experimental run temperatures used for melting the inclusions. Several melt inclusions were affected by significant overheating during experiments.

host. For experimentally heated melt inclusions, the program requires the composition of the host olivine and an independent estimate of the FeO_t content of the initial trapped melt inclusion (see Danyushevsky et al. 2000 for a description of the numerical modelling used in the program). The underlying assumption for this correction procedure is that the composition of the host olivine did not change after trapping of the melt inclusion.

In order to estimate the FeO_t content of the inclusion at the time of trapping, we calculated a liquid composition that would be in equilibrium with the host olivine, assuming the whole rock composition of sample 12009 as the parental melt. Green et al. (1971) performed phase experiments on both natural and synthetic analogues of sample 12009. Their results showed that the bulk composition of sample 12009 existed as a liquid at or close to the lunar surface and that this sample represents the best candidate for a parental magma to the Apollo 12 olivine basalt suite. Using the whole rock composition of sample 12009 as the starting melt composition, olivine fractionation trends were calculated using the olivine-melt equilibria model of Ford et al. (1983) with an oxygen fugacity 2 log units below the iron-wüstite (IW) buffer. Results of the modelling show the trapped melt in equilibrium with host olivine compositions (Fo_{75} to Fo_{46}) would have FeO_t concentrations ranging from 21 to 16 wt%. Reconstructed equilibrium trapped melt compositions and corresponding trapping temperatures were calculated for all melt inclusions (Tables 2a, 2b). This correction produced melt inclusion compositions with a relatively narrow range of K_D 's that are consistent with experimentally determined values (0.32 to 0.39; Fig. 4). PETROLOG was used to calculate the liquid line of descent for fractionating low-Ti mare lavas using the composition of sample 12009 as the starting composition. The following mineral-melt equilibria models

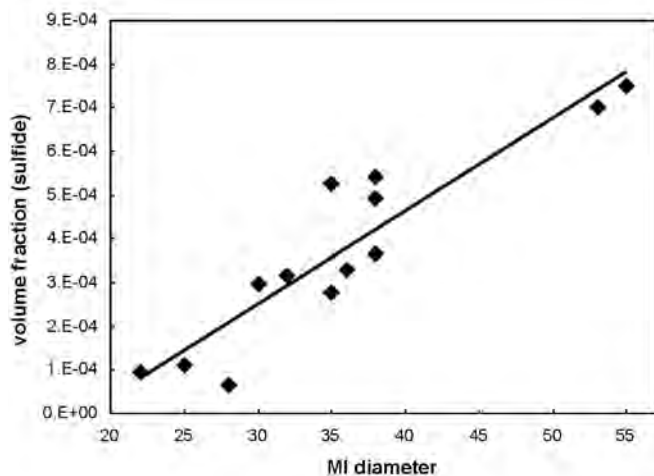


Fig. 6. The positive correlation ($R^2 = 0.85$) between proportion of sulfide in the inclusion and the size of the experimentally heated melt inclusion suggests that sulfides are not trapped primary magmatic phases but rather a consequence of sulfide saturation during heating induced by Fe loss from the inclusion to the host olivine.

were used in these calculations: Ford et al. (1983) for olivine; Ariskin et al. (1986) for clinopyroxene; Ariskin et al. (1993) for pigeonite; Ariskin and Nikolaev (1996) for spinel; Drake (1975) for plagioclase; and Nielson (1985) for ilmenite. Pressure was fixed at 0.01 kb.

Sulfur Concentrations and Immiscible Sulfides

Sulfur contents of the experimentally homogenized melt inclusions show a large range (500–1200 ppm) compared to the whole rocks (400–600 ppm; Gibson et al. 1975, 1976). Fe-Mg exchange with the host olivine lowers the FeO content of the melt and results in sulfide saturation and precipitation of sulfide globules in the melt inclusions during the heating experiments (Fig. 1c, 1d; Danyushevsky et al. 2002). Evidence that many of the sulfide globules identified in these melt inclusions are secondary and formed as a consequence of Fe loss from the melt rather than trapped primary magmatic sulfides is shown by the positive correlation ($R^2 = 0.85$) between the size of the sulfide globule and the volume of the melt inclusion (Fig. 6). The lack of visible sulfide globules in melt inclusions from sample 12035 is attributed to the elevated FeO concentrations of these inclusions (23–30 wt%). Measured sulfur contents in melt inclusions that experienced Fe loss (i.e., melt inclusions containing sulfides) will have artificially low S contents compared to their initial values at the moment of trapping. To overcome this effect and to provide an estimate of the magmatic S content of an inclusion, the compositions of melt inclusions containing sulfides were recalculated by converting sulfide and melt inclusion volumes into mass proportions and summing the relative compositions. This calculation required estimates of lunar

sulfide and melt densities, which were taken to be 4.8 and 3.2 g/cm³, respectively (Walker et al. 1976b). Mass balance was then used to calculate the total sulfur content. These recalculated compositions suggest that the primary S contents of these lavas ranged from ~700 to 1200 ppm, up to a factor of two greater than the corresponding whole rock compositions for this suite (400 to 600 ppm S; Gibson et al. 1975, 1976). The range of S concentrations in melt inclusions hosted in primitive olivine (Fo_{73–75}) may be attributed to variable degassing during transit of the magma through the lunar crust and after eruption.

Two experimentally heated melt inclusions (12020MI-5a and 12020MI-6a) contain exposed sulfide globules ~2 microns in diameter. The Fe, Ni, and S contents of these globules were measured using the electron microprobe with a focused beam. The low totals of these analyses (Table 3) probably reflect beam overlap between globules and glass in the host inclusion. Results normalized to 100% show that these globules in both samples are FeNiS, consistent with a high-temperature origin during experimental reheating. Interstitial sulfide observed in thin sections of these samples were analyzed by EMP and determined to be stoichiometric troilite (FeS), lacking Ni (Table 3).

DISCUSSION

The Apollo 12 olivine basalts have major element compositions that can be related by olivine accumulation. Walker et al. (1976a, b) found that this suite of basalts showed a strong correlation between normative olivine content (index of differentiation) and plagioclase grain size (index of cooling history; Fig. 7), and that these samples may represent the basal portion of a cooling lava flow. The initial liquid composition of the flow is represented by the sample 12009 with other members of the suite representing cumulates formed by olivine settling into the base of the flow (Walker et al. 1976b). Rhodes et al. (1977) showed that the Apollo 12 pigeonite basalts were derived from parental magmas similar in composition to the Apollo 12 olivine basalts, and so represent residual liquids complementary to the olivine cumulates.

As a test of this general petrogenetic model for Apollo 12 olivine and pigeonite basalts, corrected melt inclusion compositions were compared with modelled liquids, derived from a fractionating parental magma having a bulk composition like that of 12009 using the computer program PETROLOG (Danyushevsky et al. 2001). Major element versus MgO variation diagrams illustrate the results of the modelling (Fig. 8). Whole rock compositions of the Apollo 12 pigeonite basalts fall along the calculated fractionation trends, confirming the applicability of the computer modelling.

Major element compositions of corrected melt inclusions hosted in early-crystallized olivine (Fo_{74–75}) are almost identical to the whole rock composition of 12009 (Table 4). This supports the notion that the composition of the parent

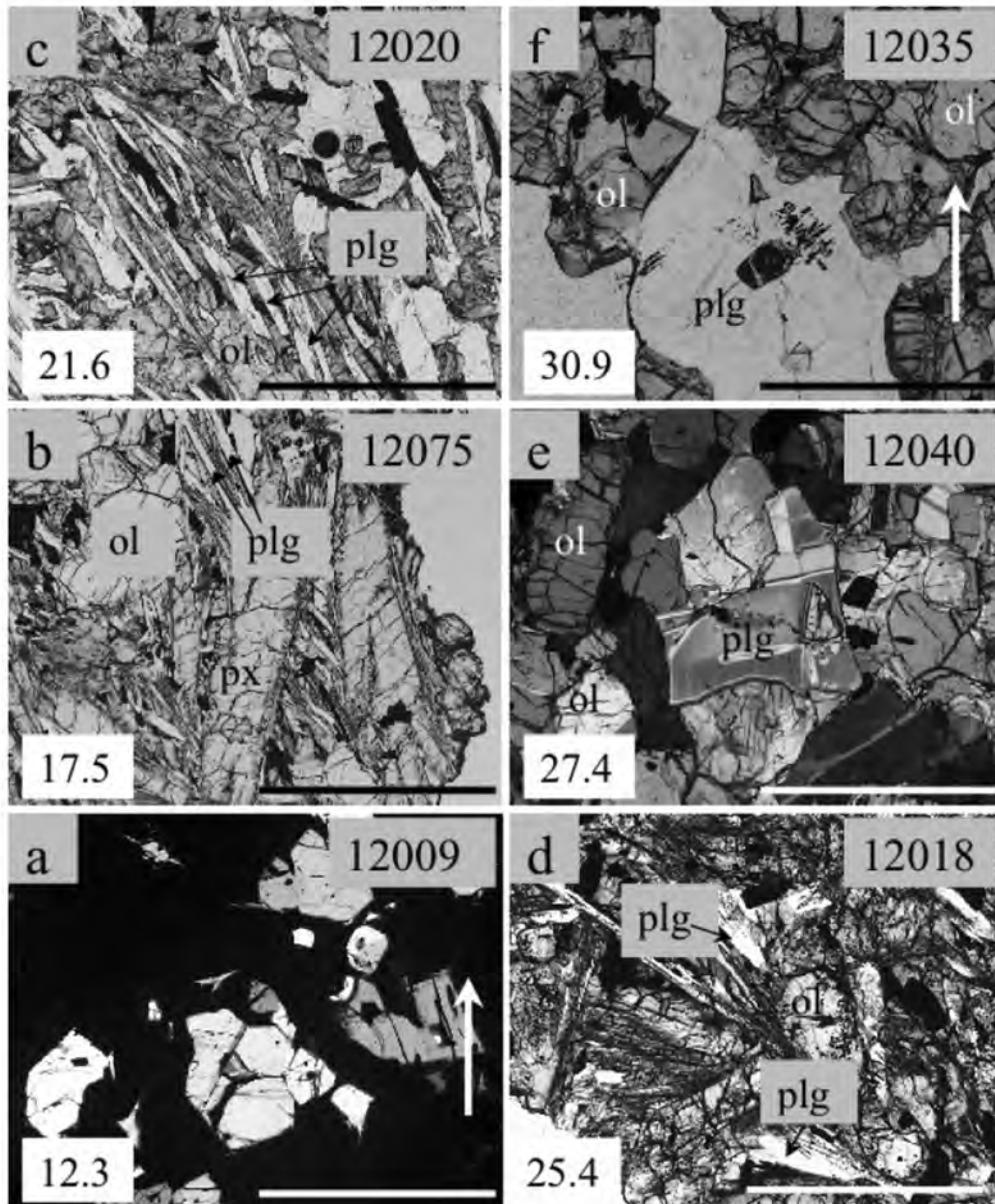


Fig. 7. Photomicrographs (transmitted light) of the Apollo 12 olivine basalt suite. In the olivine accumulation model (Walker et al. 1976a, b) increasing plagioclase grain size with increasing normative olivine content (value given in bottom left corner of each panel) demonstrates a correlation between cooling rate and extent of olivine accumulation. Arrows indicate the sequence away from the base of the flow with sample 12009 representing the initial liquid composition and 12035 the most evolved cumulate (interior of the flow). Scale bars are 1 mm.

liquid into which olivine accumulated to form the Apollo 12 picritic basalt suite was similar to the composition of 12009. For all major elements, corrected compositions of melt inclusions from samples 12009, 12075, and 12020 generally fall along the model crystallization trends. In contrast, the corrected major element concentrations of melt inclusions from samples 12018, 12040, and 12035 are characterized by higher SiO_2 , and lower Al_2O_3 and TiO_2 compared to the other samples and the calculated fractionation trends (Fig. 8). Melt inclusions from the more evolved samples appear to show

compositional variations that cannot be explained by simple crystal fractionation.

Based on the similarity of corrected melt inclusion compositions to predicted crystallization trends, samples 12009, 12075, and 12020 appear related to a common fractionating magma, thereby partially confirming the olivine accumulation model. The distinctive major element compositions of melt inclusions in 12018, 12040, and 12035 suggest that these samples may have incorporated a more evolved component prior to the crystallization of olivine, or

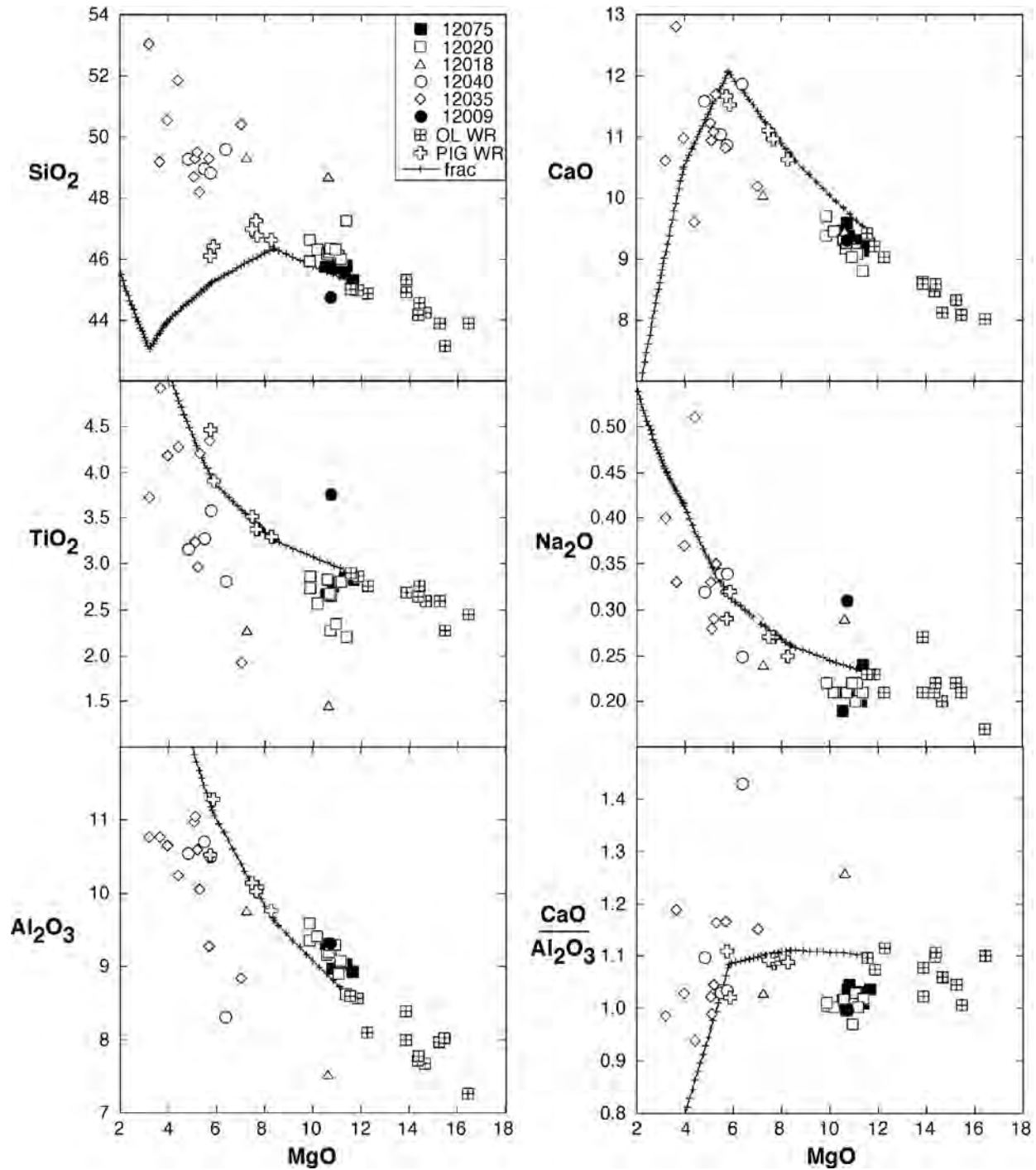


Fig. 8. MgO versus major element contents of experimentally heated, olivine-hosted melt inclusions from the Apollo 12 olivine basalt suite compared with modelled liquid compositions produced by crystal fractionation from a parent liquid similar in composition to 12009. Major element compositions of the Apollo 12 olivine and pigeonite basalts are shown to illustrate the applicability of the model fractional crystallization trend.

that these samples crystallized from compositionally distinct liquids representing different flow units. Therefore, samples 12018, 12040, and 12035 may not belong to a suite of strictly co-genetic lavas, as implied by the olivine accumulation model (Walker et al. 1976b). Finally, there remains a possibility that differences between corrected melt inclusion

compositions and model crystallization trends, particularly in more evolved melt inclusion compositions reflect; 1) uncertainties in the PETROLOG melt-equilibria models as applied to lunar compositions; 2) differences in the initial FeO_t contents compared to the assumed starting compositions, and 3) a change in the composition of the host

Table 3. Measured and corrected compositions for sulfides in melt inclusions and interstitial sample material

Sulfides	Globules in melt inclusions			Interstitial				
	12020MI-5a	12020MI-6a	12020	12040	12040	12075		
Element wt%	M	C	M	C				
S	19.91	29.29	17.62	29.83	35.66	35.79	36.00	33.00
Mn	0.06	0.08	0.08	0.13	0.00	0.01	0.00	0.00
Fe	42.31	62.25	34.02	57.61	61.51	61.39	62.64	64.22
Co	0.23	0.33	0.17	0.29	0.05	0.06	0.00	0.07
Ni	5.29	7.79	7.05	11.94	0.47	0.88	0.00	0.04
Cu	0.17	0.26	0.11	0.19	0.07	0.00	0.00	0.02
Total	67.97 ¹	100.00 ²	59.06 ¹	100.00 ²	97.76	98.12	98.64	97.36
Cation amounts								
S	42.06		42.76		50.02	50.02	50.02	47.18
Mn	0.07		0.11		0.00	0.00	0.00	0.00
Fe	51.32		47.41		49.53	49.26	49.98	52.72
Co	0.26		0.22		0.04	0.04	0.00	0.06
Ni	6.11		9.35		0.36	0.68	0.00	0.04
Cu	0.19		0.14		0.05	0.00	0.00	0.01
Sulfide	FeNiS		FeNiS		Troilite	Troilite	Troilite	Troilite

Abbreviations: Totals¹: low measured totals due to beam overlap; Totals²: measured totals normalized to 100%.

Table 4. Parental melt compositions for melt inclusions, whole rock, and experimental liquids.

Oxide wt%	MIs ¹	12009 ²	12002 ³
	Fo ₇₅	WR	Fo ₇₆
SiO ₂	45.83	45.03	43.7
TiO ₂	2.87	2.9	2.88
Al ₂ O ₃	8.99	8.59	8.22
FeO	20.98	21.03	21.8
MnO	0.15	0.28	0.35
MgO	11.23	11.55	12.5
CaO	9.15	9.42	8.39
Na ₂ O	0.23	0.23	n.d.
K ₂ O	0.07	0.06	0.07
P ₂ O ₅	0.09	0.07	n.d.
Cr ₂ O ₃	0.39	0.55	0.83
Total	100.00	99.71	98.74
mg#	48.8	49.5	50.5

Abbreviations: MIs¹ = an average of seven analyses of melt inclusion compositions hosted in early formed olivine (Fo₇₄₋₇₅); 12009² = sample 12009 (parent liquid) whole rock composition (Papike et al. 1999); 12002³ = experimentally determined liquid composition (sample 12002) in equilibrium with olivine Fo₇₆ (Walker et al. 1976a).

olivine after trapping of the melt inclusion producing an incorrect host olivine composition as input to the Fe-loss correction procedure. Uncertainties such as these are presently difficult to quantify.

Primary S Abundances in Apollo 12 Olivine Basalts

Some mare lavas are believed to have lost large amounts of sulfur and other volatile species (e.g., CO) through degassing during transport to the lunar surface and exposure to the hard vacuum of space (Weitz et al. 1999). When these lavas finally crystallized, they did so with lower concentrations of volatiles than initially present in the melt.

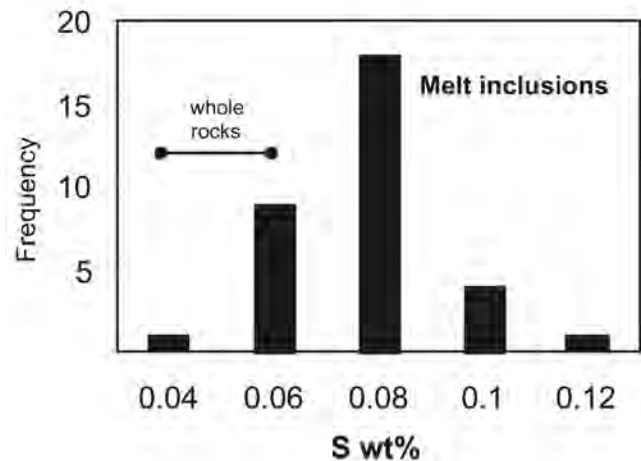


Fig. 9. Histogram of recalculated S contents in olivine-hosted melt inclusions (this study) compared to whole rock values (Gibson et al. 1975, 1976).

This general view of mare basalt evolution is supported by measured S contents in the Apollo 12 melt inclusions, which are a factor of two greater than their whole rock equivalents (Fig. 9). The identity of the outgassing species has not been positively identified, although the reduced species COS would be consistent with the low oxygen fugacity of mare lavas (Sato 1976; Carroll and Webster 1994).

If the Apollo 12 picritic magmas lost most of their volatiles after olivine crystallization began, melt inclusions trapped in near-liquidus olivine (Fo₇₅) should provide better estimates for primary sulfur contents of Apollo 12 basaltic magmas than whole rock compositions. Sulfur contents of melt inclusions hosted in Fo₇₃₋₇₅ olivine range from 850 to 1053 ppm (Fig. 9). The range of S contents in these primitive olivines may be attributed to variable outgassing during

transit of the magma through the lunar crust and after eruption. Based on the melt inclusion compositions, we propose that the primary S content of the magma parental to the Apollo 12 olivine basalts was ≥ 1050 ppm.

Sulfide Saturation in the Apollo 12 Mare Basalts

No direct sample of the lunar mantle has yet been discovered, whether by Apollo astronauts or from recovered meteorites. Therefore, estimates of chalcophile element abundances (Cu, PGE, Au) in the lunar mantle must be inferred indirectly from the compositions of erupted mare lavas. By definition, chalcophile elements have a strong affinity for sulfide phases, and the concentrations of these elements in primitive terrestrial basalts are largely controlled by the presence or absence of sulfides in the upper mantle during melting (Mathez et al. 1976; Peach et al. 1990; Keays et al. 1995). For example, low concentrations of chalcophile elements in MORB and OIB have been attributed at least in part to the retention of sulfides in their mantle source regions (Rehkamper et al. 1997; Richter and Hauri 1998; Roy-Barman et al. 1998; Bennett et al. 2000). Despite the potential importance of mantle sulfides for understanding the chalcophile element composition of the Moon, few studies have considered the implications of sulfide saturation in mare basalt source regions (Gibson et al. 1975, 1976; Brett et al. 1976; Richter et al. 2000).

Numerous experimental studies have been performed to determine the sulfur solubility limit (SSL) for basaltic melt compositions (Haughton et al. 1974; Shima and Naldrett 1975; Carroll and Rutherford 1979; Danckwerth et al. 1979; Wendlandt 1982; Wallace and Charnicheal 1991; Mavrogenes and O'Neill 1999; Holzheid and Grove 2002; O'Neill and Mavrogenes 2002) and also for synthetic alumino-silicate systems (Fincham and Richardson 1954). The latter provided important information on the mechanism of sulfur solution and showed that at low oxygen fugacities, sulfur dissolves in silicate melts primarily as sulfide. Furthermore these studies established that the Fe content of the melt, temperature, melt composition, oxygen and sulfur fugacity as well as pressure are all important parameters, which control the ability of a melt to dissolve sulfur.

Previous experimental studies of S solubility were designed primarily with parameter values relevant for terrestrial melts. However, lunar melts formed and crystallized under markedly different compositions. For example, compared to terrestrial basaltic magmas, mare basalts are enriched in FeO by a factor of 2. Oxygen fugacity of lunar basaltic magmas, at equivalent terrestrial temperatures, is ~ 2 log units below the iron-wüstite (IW) buffer, whereas oxygen fugacities for terrestrial basalts lie near the FMQ buffer (BSVP 1981). These differences (low ratios of f_{O_2}/f_{S_2} and high FeO contents) suggest lunar melts have a great capacity to dissolve sulfur. For example, sulfur

solubility experiments conducted on high-Ti basaltic magma compositions at 1 atm show these magmas require up to 3500 ppm S to achieve sulfide saturation (Danckwerth et al. 1979). Sulfur solubility experiments by Haughton et al. (1974) at 1 atm show that basaltic compositions approaching Apollo 12 low-Ti magmas required ~ 2000 ppm S to achieve sulfide saturation.

It is difficult to estimate the sulfide saturation limit (SSL) for low-Ti magmas at pressures of between 10 to 12.5 kb, where such magmas were generated (Snyder et al. 1997) because experiments on pressure and its effect on the SSL for lunar basaltic compositions have not been conducted. Furthermore the effect of pressure on the SSL of terrestrial basaltic compositions is controversial. For example, recent studies have shown that the sulfur content of a melt saturated with sulfide increases with decreasing pressure, so that a melt becomes further removed from sulfide saturation as it migrates toward the surface (Wendlandt 1982; Mavrogenes and O'Neill 1999; Holzheid and Grove 2002). Other investigations have found the opposite effect, or suggest that decreasing temperature during magma ascent will negate the effects of pressure on sulfur solubility (Mysen and Popp 1980; Naldrett 1989). Taking into account the low lunar pressure gradient, we expect that the effect of pressure on the SSL of Apollo 12 low-Ti magmas will be minimal and do not consider it further.

Experimental studies by Haughton et al. (1974) into sulfur solubility at 1 atm show that compositions of magmas approaching those of Apollo 12 low-Ti basalts would require ~ 2000 ppm S to achieve sulfide saturation. Unless the Apollo 12 picritic magmas experienced significant (factor of 2) S loss prior to crystallization of the liquidus olivines, it appears unlikely these melts were saturated with sulfide in their mantle source regions. The absence of primary magmatic sulfide globules from both the matrix of sample 12009 and in early-formed olivine phenocrysts supports this inference. As Apollo 12 low-Ti magmas migrated toward the lunar surface, they remained sulfide undersaturated, and would have carried most of the mantle budget of incompatible chalcophile elements. Therefore, the low abundances of chalcophile elements in low-Ti mare basalts must be a primary feature of the lunar mantle and not the result of sulfide saturation during melting.

The S Content of Apollo 12 Mare Basalt Source Regions

Estimates for the concentration of S in the lunar mantle are not well constrained. Using results from this study along with previous investigations, we can estimate the amount of sulfur present in Apollo 12 mare source regions using the batch melting equation $C_o = C_L [D_o + F (1-D_o)]$, where C_o = concentration of the element in the initial cumulate solid; C_L = concentration of an element in the derivative melt; F = fraction of melt produced; D_o = bulk mineral/melt distribution coefficient. High-pressure phase experiments

along with trace element analysis show a parental basalt similar in composition to sample 12009 can be generated by between 7% to 10% melting of an olivine-pyroxenite source at depths between 100–250 km (equivalent to 5–13 kb; Green et al. 1971; Neal et al. 1994a, b; Snyder et al. 1997). For the purpose of this exercise we make the following assumptions: 1) no residual sulfide is present during melting thus making S behave as a perfectly incompatible element. Therefore, the bulk mineral/melt distribution coefficient D_0 equals zero; 2) melt inclusions hosted in early formed olivine represent the primary S content of the parental melt (this study). Therefore, the concentration of sulfur in the derivative melt C_L equals 1050 ppm. For 7% melting of an olivine-pyroxenite source, the concentration of sulfur in the initial cumulate solid C_0 would equal 75 ppm, thereby providing an estimate of the sulfur content of the Apollo 12 mare basalt source region. If the Apollo 12 olivine basalt parental magma lost S prior to the crystallization of olivine with composition FO_{75} , the amount of S in the source region would be correspondingly higher. The Apollo 12 mare basalt source region appears to have had a S content that was a factor of 2–3 less than that of the Earth's upper mantle (250 ppm; McDonough and Sun 1995). Such S contents may be consistent with the volatile-depleted nature of the Moon relative to the earth, or loss of S to a lunar core.

CONCLUSIONS

Trends observed in corrected major element compositions of melt inclusions from Apollo 12 olivine basalt samples 12009, 12075, and 12020 reflect fractional crystallization of a parental melt composition similar in composition to that of sample 12009, thereby partially confirming the olivine accumulation model proposed by Walker et al. (1976). In contrast, melt inclusions from samples 12018, 12040, and 12035 appear to have crystallized from melts compositionally distinct from the 12009 parent liquid, and may not be strictly cogenetic with other members of the Apollo 12 olivine basalt suite.

The parental magma of the Apollo 12 olivine basalts contained ≥ 1050 ppm S and experienced significant outgassing and loss of at least half of its primary S content during cooling and crystallization. This magma was undersaturated in sulfide as the melt left its source region, and thus it must have transported incompatible chalcophile elements from the lunar mantle to the surface. Therefore, the low concentrations of chalcophile elements in low-Ti mare basalts are a primary feature of the lunar mantle, and not the result of residual sulfide remaining in the mantle during melting. The sulfur content of the Apollo 12 mare basalt source region is estimated to be ~ 75 ppm, considerably less than that of the terrestrial upper mantle.

Acknowledgments—We thank the crew of Apollo 12, the NASA Planetary Materials Curatorial Laboratories at the

Johnston Space Center, Houston, for supplying lunar samples. We thank David Steele for assistance with electron microprobe analyses, Maya Kamenetsky for help with sample preparation, and the Australian Research Council and University of Tasmania for support of this project. We also thank Dr. Clive Neal and Dr. Mac Rutherford for helpful comments during the review process.

Editorial Handling—Dr. Randy Korotev

REFERENCES

- Ariskin A. A., Barmina G. S., and Frenkel M. Ya. 1986. Simulating low-pressure tholeiite-magma crystallization at a fixed oxygen fugacity. *Geokhimiya* 11:1614–1627; *Geochemica International* 24:92–100. Translated into English in 1987.
- Ariskin A. A., Frenkel M. Ya., Barmina G. S., and Nielsen R. 1993. COMAGMAT: A Fortran program to model magma differentiation processes. *Computers & Geosciences* 19:1155–1170.
- Ariskin A. A. and Nikolaev G. S. 1996. An empirical model for the calculation of spinel-melt equilibria in mafic igneous systems at atmospheric pressure: 1. Chromian spinels. *Contributions to Mineralogy and Petrology* 123:282–292.
- Basalt Volcanism Study Project. 1981. *Basalt volcanism on the terrestrial planets*. New York: Pergamon Press. 1286 p.
- Bennett V. C., Norman M. D., and Garcia M. 2000. Rhenium and platinum-group element abundances correlated with mantle source components in Hawaiian picrites: Sulphides in the plume. *Earth and Planetary Science Letters* 183:513–526.
- Brett R. 1976. Reduction of mare basalt by sulfur loss. *Geochimica et Cosmochimica Acta* 40:997–1004.
- Carroll M. R. and Rutherford M. J. 1985. Sulfide and sulfate saturation in hydrous silicate melts. Proceedings, 15th Lunar and Planetary Science Conference. pp. C601–C612.
- Carroll M. R. and Webster J. D. 1994. Solubilities of sulfur, noble gases, nitrogen, chlorine, and fluorine in magmas. In *Volatiles in magmas*, edited by Carroll M. R. and Holloway J. R. Washington D.C.: Mineralogical Society of America. pp. 231–279.
- Danckwerth P. A., Hess P. C., and Rutherford M. J. 1979. The solubility of sulphur in high-TiO₂ mare basalts. Proceedings, 10th Lunar and Planetary Science Conference. pp. 517–530.
- Danyushevsky L. V., Della-Pasqua F. N., and Sokolov S. 2000. Re-equilibration of melt inclusions trapped by magnesian olivine phenocrysts from subduction-related magmas: Petrological implications. *Contributions to Mineralogy and Petrology* 138: 68–83.
- Danyushevsky L. V. 2001. The effects of small amounts of H₂O on crystallization of mid-ocean ridge and backarc basin margins. *Journal of Volcanology and Geothermal Research* 110:265–280.
- Danyushevsky L. V., McNeill A. W., and Sobolev A. V. 2002. Experimental and petrological studies of melt inclusions in phenocrysts from mantle derived magmas: An overview of techniques, advantages and complications. *Chemical Geology* 183:5–24.
- Drake M. J. 1976. Plagioclase-melt equilibria. *Geochimica et Cosmochimica Acta* 40:457–465.
- Fincham C. J. B. and Richardson F. D. 1954. The behavior of sulfur in silicate and aluminate melts. *Proceedings of the Royal Society of London A* 223:40–62.
- Ford C. E., Russel D. G., Craven J. A., and Fisk M. R. 1983. Olivine-liquid equilibria: Temperature, pressure and composition dependence of the crystal/liquid cation partition coefficients for

- Mg, Fe²⁺, Ca and Mn. *Journal of Petrology* 24:256–265.
- Gibson E. K., Jr., Chang S., Lennon K., Moore G. W., and Pearce G. W. 1975. Sulfur abundances and distributions in mare basalts and their source magmas. Proceedings, 6th Lunar Science Conference. *Geochimica et Cosmochimica Acta, Supplement 6*: 1287–1301.
- Gibson E. K., Jr., Morris R. V., and Usselman T. M. 1976. Sulfur abundances in the Apollo 17 basalts and its role in their source. Proceedings, 7th Lunar Science Conference. *Geochimica et Cosmochimica Acta, Supplement 6*:1491–1505.
- Green D. H., Ringwood A. E., Ware N. G., Hibberson W. O., and Major A. 1971. Experimental petrology of Apollo 12 basalts: Pt. 1, Sample 12009. *Earth and Planetary Science Letters* 13:85–96.
- Haughton D., Roedder P. L., and Skinner B. J. 1974. Solubility of sulfur in mafic magmas. *Economic Geology* 69:451–467.
- Holzheid A. and Grove T. L. 2002. Sulphur saturation limits in silicate melts and their implications for core formation scenarios for terrestrial planets metal. *American Mineralogist* 87:227–237.
- Jaroswich E. J., Nelen J. A., and Norberg J. A. 1979. Reference sample for electron microprobe analysis. *Geostandards Newsletter* 4:43–47.
- Keays R. R. 1995. The role of komatiitic and picritic magmatism and S-saturation in the formation of ore deposits. *Lithos* 34:123–145.
- Mathez E. A. 1976. Sulfur solubility and magmatic sulfides in submarine basaltic glasses. *Journal of Geophysical Research* 81: 4269–4276.
- Mavrogenes J. A. and O'Neill H. St. C. 1999. The relative effects of pressure, temperature and oxygen fugacity on the solubility of sulfide in mafic magmas. *Geochimica et Cosmochimica Acta* 63: 1173–1180.
- Mysen B. O. and Popp R. P. 1980. Solubility of sulfur in CaMgSi₂O₆ and NaAlSi₃O₈ melts at high pressure and temperature with controlled fO₂ and fS₂. *American Journal of Science* 280:78–92.
- Naldrett A. J. 1989. *Magmatic sulfide deposits*. New York: Clarendon Press. 186 p.
- Neal C. R., Hacker M. D., Snyder G. A., Taylor L. A., Liu Y.-G., and Schmitt R. A. 1994a. Basalt generation at the Apollo 12 site, Part 1. New data, classification, and re-evaluation. *Meteoritics & Planetary Science* 29:334–348.
- Neal C. R., Hacker M. D., Snyder G. A., Taylor L. A., Liu Y.-G., and Schmitt R. A. 1994b. Basalt generation at the Apollo 12 site, Part 2. Source heterogeneity, multiple melts, and crustal contamination. *Meteoritics & Planetary Science* 29:349–361.
- Nielsen R. L. 1985. EQUIL: A program for the modelling of low-pressure differentiation processes in natural mafic magma bodies. *Computers and Geosciences* 11:531–546.
- O'Neill H. St. C. and Mavrogenes J. A. 2002. The sulfide capacity and the sulfur content at sulfide saturation of silicate melts at 1400 °C and 1 bar. *Journal of Petrology* 43:1049–1087.
- Papike J. J., Fowler G. W., Adcock C. T., and Shearer C. K. 1999. Systematics of Ni and Co in olivine from planetary melt systems: Lunar mare basalts. *American Mineralogist* 84:392–399.
- Peach C. L., Mathez E. A., and Keays R. R. 1990. Sulfide melt-silicate melt distribution coefficients for the noble metals and other chalcophile metals as deduced from MORB. Implications for partial melting. *Geochimica et Cosmochimica Acta* 54:3379–3389.
- Rehkamper M., Halliday A. N., Barfod D., and Fitton J. G. 1997. Platinum-group element abundance patterns in different mantle environments. *Science* 278:1595–1598.
- Rhodes J. M., Blanchard D. P., Dungan M. A., Brannon J. C., and Rodgers K. V. 1977. Chemistry of Apollo 12 of mare basalts: Magma types and fractionation processes. Proceedings, 8th Lunar Science Conference. pp. 1751–1765.
- Righter K. and Hauri E. H. 1998. Compatibility of rhenium in garnet during mantle melting and magma genesis. *Science* 280:1737–1741.
- Righter K., Walker J. R., and Warren P. H. 2000. Significance of highly siderophile elements and osmium isotopes in the lunar and terrestrial mantles. In: *Origin of the Earth and the Moon*, edited by R. M. Canup and K. Righter. Tucson, Arizona: The University of Arizona Press. pp. 291–322.
- Roedder E. 1979. Origin and significance of magmatic inclusions. *Bulletin Minéralogique* 102:487–510.
- Roy-Barman M., Wasserburg G. J., Papanastassiou D. A., and Chaussidon M. 1988. Osmium isotopic compositions and Re-Os concentrations in sulfide globules from basaltic glasses. *Earth and Planetary Science Letters* 154:331–347.
- Sato M., Hickling N. L., and McLane J. E. 1976. Oxygen fugacity values of Apollo 12, 14, 15 lunar samples and reduced state of lunar magmas: Proceedings, 4th Lunar Science Conference. *Geochimica et Cosmochimica Acta, Supplement 4*:1061–1079.
- Shima H. and Naldrett A. J. 1975. Solubility of sulfur in an ultramafic melt and the relevance of the system Fe-S-O. *Economic Geology* 70:960–967.
- Snyder A. G., Neal C. R., Taylor A. L., and Halliday N. A. 1997. Anatexis of lunar cumulate mantle in time and space. Clues from trace element, strontium, and neodymium isotopic chemistry of parental Apollo 12 basalts. *Geochimica et Cosmochimica Acta* 61:2731–2747.
- Sobolev A. V., Dmitriev L. V., Barsukov V. L., Nevsorov V. N., and Slutsky A. B. 1980. The formation conditions of the high-magnesium olivines from the monomineralic fraction of Luna 24 regolith. Proceedings, 11th Lunar and Planetary Science Conference. pp. 105–116.
- Sobolev A. V. 1996. Melt inclusions in minerals: A source of principle petrological information. *Petrologiya* 4:228–239.
- Walker D., Kirkpatrick R. T., Longhi J., and Hays J. F. 1976a. Crystallisation history of lunar picritic basalt sample 12002: Phase-equilibria and cooling rate studies. *Geological Society of America Bulletin* 87:646–656.
- Walker D., Longhi J., Kirkpatrick R. J., and Hays J. F. 1976b. Differentiation of an Apollo 12 picrite magma. Proceedings, 7th Lunar Science Conference. pp. 1365–1389.
- Wallace P. and Carmichael I. S. E. 1991. Sulfur in basaltic magmas. *Geochimica et Cosmochimica Acta* 56:1863–1874.
- Weiblen P. W. 1977. Examination of the liquid line of descent of mare basalts in light of data from melt inclusions in olivine. Proceedings, 8th Lunar Science Conference. pp. 1751–1765.
- Wendlandt R. F. 1982. Sulfide saturation of basaltic melts at high pressures and temperatures. *American Mineralogist* 67:877–885.
- Weitz C. M., Rutherford M. J., Head J. W., III, and McKay D. S. 1999. Ascent and eruption of a lunar high-titanium magma as inferred from the petrology of the 74001/2 drill core. *Meteoritics & Planetary Science* 34:527–540.